NeuroImage xxx (2009) xxx–xxx

Contents lists available at ScienceDirect

NeuroImage

journal homepage: www.elsevier.com/locate/ynimg

In vivo cerebromicrovasculatural visualization using 3D ΔR_2-based microscopy of magnetic resonance angiography (3DΔR_2-mMRA)

Chien-Yuan Lin [a,b], Ming-Huang Lin [b], Wai-Mui Cheung [b], Teng-Nan Lin [b], Jyh-Horng Chen [a,*], Chen Chang [b,*]

[a] Interdisciplinary MRI/MRS Lab, Department of Electrical Engineering, National Taiwan University, Taipei, Taiwan, ROC
[b] Institute of Biomedical Sciences, Academic Sinica, Taipei, Taiwan, ROC

ARTICLE INFO

Article history:
Received 11 September 2008
Revised 13 November 2008
Accepted 8 December 2008
Available online xxxx

ABSTRACT

This study proposed a novel methodology for depicting cerebral small vessels including veins, arterioles, and venules, called 3DΔR_2-mMRA (three-dimensional, steady-state ΔR_2-based, and flow-independent microscopic magnetic resonance angiography). The ΔR_2 map calculated by a fast spin-echo imaging technique before and after the injection of an iron-oxide contrast agent was used to delineate the relative cerebral blood volume, primarily to microvasculature. The proposed 3DΔR_2-mMRA method, which employs 3D reconstruction techniques, can simultaneously provide high-resolution 3D information on the cerebral anatomy, in vivo microvascular architecture, and hemodynamic response, which can be used to evaluate pathological microvascular changes over time in cerebromicrovascular disease. Since spin-echo-based ΔR_2 imaging was applied, the inflow effects, susceptibility artifacts, and the overestimation of vessel size in brain were reduced. A well-defined three-vessel occlusion model in the rat was performed to evaluate the capability of the proposed method in evaluating alterations to the microvasculature.

Introduction

The normal function and structure of microvessels are crucial to the survival of tissue cell due to essential nutrients passing through their walls. Structural and functional cerebromicrovascular abnormalities are implicated in the pathogenesis of brain diseases (Perlmutter and Chui, 1990; Buee et al., 1997; Serne et al., 2007). Imaging methods for assessing the cerebromicrovasculature is therefore important in a wide range of clinical and neuroscience-research fields. The most commonly used magnetic resonance (MR) angiography (MRA) techniques to visualize the vasculature are time-of-flight MRA (TOF-MRA) and contrast-enhanced MRA (CE-MRA). TOF-MRA depends on the motion of water protons in inflowing blood, which is sensitive to rapidly inflowing spins (i.e., in arteries), whereas CE-MRA employs contrast agents to detect low flow rates in veins (Reese et al., 1999; Miraux et al., 2004). Combining these MRA methods with a short echo time, flow compensation, and a magnetization transfer technique could be insensitive to flow-related artifacts such as vessel dislocation, signal cancellation in areas with turbulent flow, and motion artifacts from pulsatile flow, and could improve the contrast between flowing vessels and stationary tissues (Beckmann et al., 1999; Pipe, 2001). These methods are nowadays quite suitable for detecting larger arteries or veins, and hence have been widely used to study vascular diseases such as tumor-related vasculature (van Vliet et al., 2005), transient focal ischemia (Beckmann et al., 1999; Besselmann et al., 2001), and genetic variations of the vascular structure (Beckmann, 2000; Brubaker et al., 2005). However, the vessel-related signals in TOF-MRA are naturally related to high-flow-rate vessels, and have a limited capability to visualize cerebral small vessels, especially when acquiring data with a 3D sequence (Pipe, 2001). CE-MRA with the injection of Gd-DTPA, which has a short intravascular (IV) half-life and rapidly redistributes into the extracellular space, may not satisfy the long acquisition time required for high-resolution MRA applications.

Cerebral small vessels can be imaged by an MR venography technique based on detecting the enriched-deoxyhemoglobin-induced blood-oxygenation-level-dependent (BOLD) effect in veins and venules using T2*-weighted imaging (T2*WI) (Reichenbach et al., 1997; Koopmans et al., 2008; Park et al., 2008). It describes, however, the venous vessels with negative signals that are strongly obscured by signal dephasing near the air–tissue interface. An alternative technique based on calculating the difference in contrast-agent-induced susceptibility between the pre- and postcontrast images has been proposed (Dennie et al., 1998; Bolan et al., 2006). This technique increases the difference in magnetic susceptibility between blood vessels and surrounding tissues, and it also shows both arterioles and venules as positive signals. However, evaluating contrast-agent-induced susceptibility in neural tissue is complex because it is affected by the tissue vasculature, field strength, and types of pulse sequences

* Corresponding authors. C. Chang is to be contacted at Functional and Micro-Magnetic Resonance Imaging Center, Institute of Biomedical Sciences Academia Sinica, Taipei 11529, Taiwan, ROC. Fax: +886 2 2788 7641. J.-H. Chen, Interdisciplinary MRI/MRS Lab Department of Electrical Engineering, National Taiwan University, Taipei, Taiwan ROC. Fax: +886 2 2325 9043.
E-mail addresses: chen@me.ee.ntu.edu.tw (J.-H. Chen), bmcchen@ibms.sinica.edu.tw (C. Chang).

1053-8119/$ – see front matter © 2008 Elsevier Inc. All rights reserved.
doi:10.1016/j.neuroimage.2008.12.030

and their parameters (Weisskoff et al., 1994; Boxerman et al., 1995). It has been shown that the spin-echo-based ΔR_2 is associated with the microvasculature, while gradient-echo-based ΔR_2^* is sensitive to vessels of all sizes, with both parameters being independent of blood flow (Boxerman et al., 1995). Therefore, in order to visualize cerebral small vessels and be insensitive to flow-related artifacts, we propose a new steady-state three-dimensional ΔR_2-based microscopic MRA (3DΔR_2-mMRA) method that combines high-resolution 3D ΔR_2 images with volume rendering (VR) or maximum-intensity projection (MIP) to directly visualize the cerebromicrovasculature (Drebin et al., 1988; Cai and Sakas, 1998). The ΔR_2 map, based on the measurement of the spin-echo transverse relaxation rate by a fast spin-echo (FSE) imaging technique before and after the injection of an iron-oxide contrast agent, has been commonly used to depict the microvascular cerebral blood volume (CBV), and it provides linear change with the blood volume fraction (Boxerman et al., 1995; Dunn et al., 2004). Furthermore, the spin-echo-based sequence also has the important advantage of being less extravascular dephasing and less sensitive to geometric distortion caused by magnetic field inhomogeneities at the air–tissue interface, and thus produces images of higher quality.

The proposed flow-independent 3DΔR_2-mMRA method can be used to both visualize the neuromicrovascular architecture and provide information on the physiological status of the microvascular CBV. Both a control and a well-defined three-vessel occlusion model in the rat were employed to evaluate the capabilities of the proposed 3DΔR_2-mMRA method.

Methods

Transverse relaxation rate change in spin-echo (ΔR_2) and regional CBV

The ΔR_2 value is given by (Wu et al., 2003)

$$\Delta R_2 = \frac{1}{\mathrm{TE}} \ln\left(\frac{S_{\mathrm{pre}}}{S_{\mathrm{post}}}\right) \quad (1)$$

where TE is the echo time, and S_{pre} and S_{post} are the pre- and postcontrast signal intensities, respectively. ΔR_2 varies approximately linearly with the CBV fraction; that is, $\Delta R_2 \approx k \cdot [\mathrm{CA}] \cdot \mathrm{CBV}$, where k is a constant that depends on the tissue type, pulse sequence, field

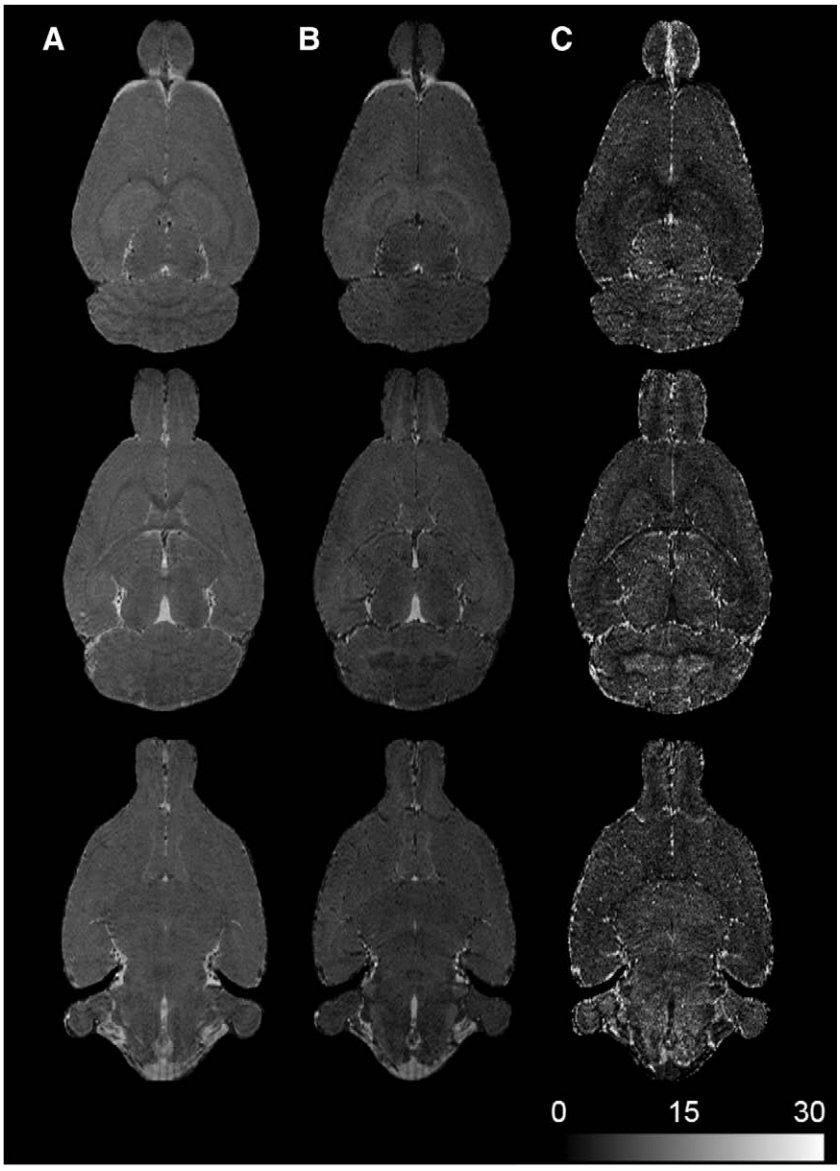

Fig. 1. High-resolution T2WI images and computed ΔR_2 maps of a rat brain. Images of different axial views were extracted from an entire 3D data set with the nominal resolution of 54×54×72 μm. (A) precontrast T2WI images, (B) postcontrast T2WI images (Resovist, 30 mg/kg), and (C) computed ΔR_2 maps.

Please cite this article as: Lin, C.-Y., et al., In vivo cerebromicrovasculatural visualization using 3D ΔR_2-based microscopy of magnetic resonance angiography (3DΔR_2-mMRA), NeuroImage (2009), doi:10.1016/j.neuroimage.2008.12.030

strength, and contrast agent, and [CA] is the concentration of the contrast agent in blood. The ΔR_2 signal consists of IV and extravascular (EV) components (Boxerman et al., 1995; Duong et al., 2003). The ΔR_2 IV signal exists in vessels of all sizes because the change in T2 value in blood is induced by the contrast agent, whereas the EV effect in spin-echo-based ΔR_2 is associated with small vessels because the 180° radiofrequency (RF) pulse refocuses the static dephasing induced by field inhomogeneities but cannot completely reverse the dephasing component induced by the diffusion effect around small vessels (Ogawa et al., 1993; Weisskoff et al., 1994; Boxerman et al., 1995). Simulations have shown that the diffusion effect is minimal for vessels larger than 20 μm (Bandettini and Wong, 1995).

Stroke model

The rat focal cerebral ischemia-reperfusion model was described by Lin et al. (1993). In brief, the right middle cerebral artery (MCA) of male Long–Evans rats was reversibly ligated under a stereomicroscope. Both common carotid arteries were then occluded using nontraumatic aneurysm clips. After 60 min of ischemia, arterial occlusion was released. The rectal temperature of anesthetized rats was maintained at 37.0 ± 0.5 °C using a homeothermic blanket (Harvard, Holliston, MA).

Data acquisition

All imaging was performed on a 4.7-T MR scanner (Biospec 47/40, Germany) equipped with an active shielding gradient (20 G/cm in 80 μs),with all experiments involving male Long–Evan rats weighing 300–350 g. Each rat was initially anesthetized with 5% isoflurane at an oxygenation rate of 1 L/min. When fully anesthetized, the animal was placed in a prone position and fitted with a custom-designed head holder inside the magnet. Isoflurane was then maintained with 1–1.2% at 1 L/min oxygenation throughout the experiments, which causes minimal cerebral hemodynamic changes (Lei et al., 2001). Images were acquired using a 72-mm birdcage transmitter coil and a separate quadrature surface coil for signal detection. To determine ΔR_2, T2-weighted imaging (T2WI) was performed before and after injecting superparamagnetic iron-oxide nanoparticles (Resovist, Schering AG, Berlin, Germany) at a dose of 30 mg Fe/kg. The postcontrast image acquisition was delayed by 1–2 min to ensure that the distribution of contrast agent in the vascular network had reached a steady state. T2WI was performed using a 3D FSE sequence with a repetition time (TR) of 1500 ms, an effective echo time (TE_{eff}) of 82 ms, a sampling bandwidth of 50 kHz, an echo-train length (ETL) of 32, 4 averages, a field of view (FOV) of 2.8 × 2.8 × 1.4 cm, an acquisition matrix of 256 × 256 × 96 (zero-padded to 512 × 512 × 192), and a total acquisition time of 76 min. The in-plane resolution and slice thickness were 54.68 and 72.91 μm, respectively. TOF-MRA was performed using FLASH (fast low-angle shot) with a TR of 30 ms, a TE of 10 ms, a flip angle of 30°, and with the same FOV and matrix size as for the 3DΔR_2-mMRA method.

Data analysis

The 3D whole-brain precontrast images were coregistered with the postcontrast images using a coregistration algorithm implemented using the function of Normalized Mutual Information with the rigid transform in Amira software (TGS, San Diego, CA), which is an easy-to-use and powerful 3D visualization platform that allows users to

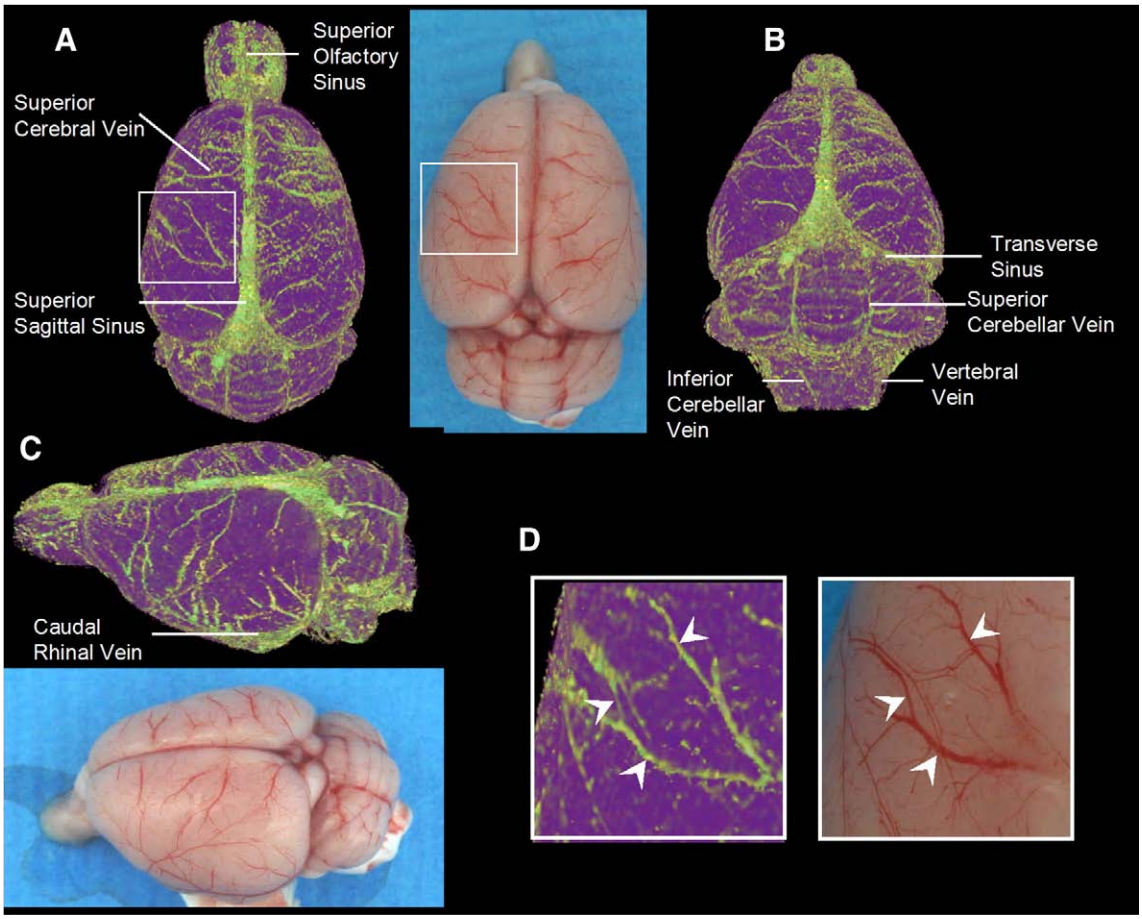

Fig. 2. 3DΔR_2-mMRA images and corresponding vascular photographs of a normal rat. (A) Dorsal bird's-eye view of 3DΔR_2-mMRA and the corresponding vascular photograph. (B) Same data set as A with a small angular tilt, highlighting the cerebellar region. (C) Lateral view of 3DΔR_2-mMRA and the corresponding vascular photograph. (D) Magnified sections of the data sets shown in A. Arrowheads indicate the vascular region where the vessel size was compared between the two methods.

Please cite this article as: Lin, C.-Y., et al., In vivo cerebromicrovasculatural visualization using 3D ΔR_2-based microscopy of magnetic resonance angiography (3DΔR_2-mMRA), NeuroImage (2009), doi:10.1016/j.neuroimage.2008.12.030

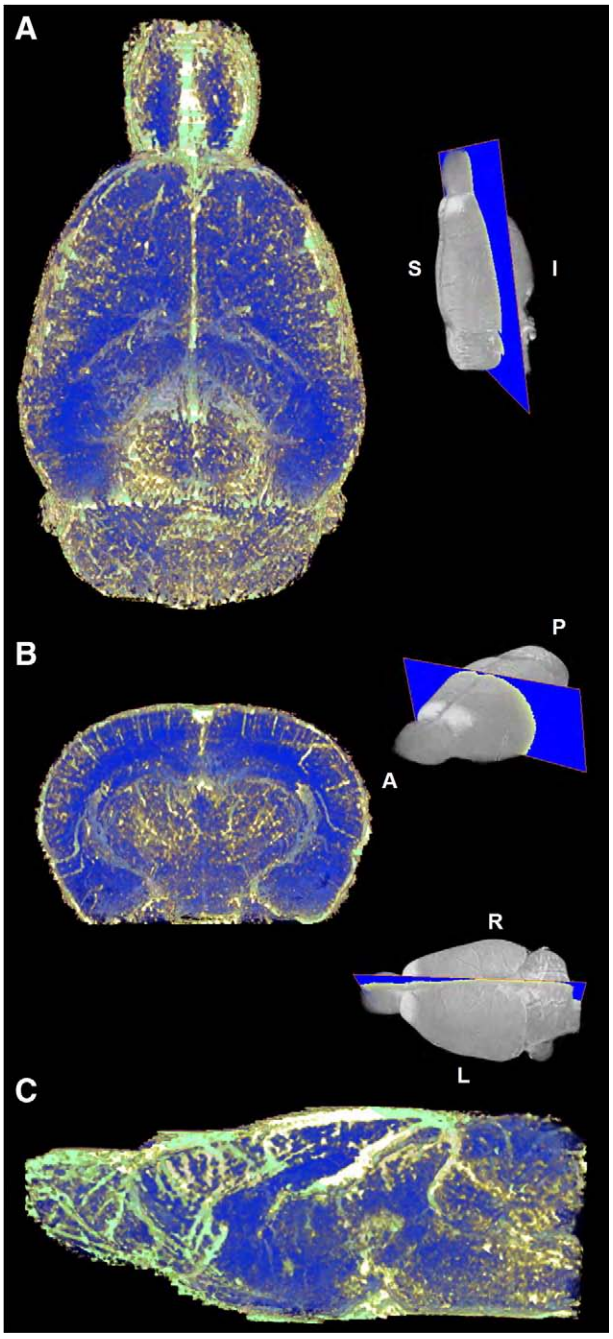

Fig. 3. VR 3DΔR_2-mMRA of a normal rat in three orthogonal views: (A) axial slice plane, superior-to-inferior view (S–I); (B) coronal slice plane, anterior-to-posterior view (A–P); and (C) sagittal slice plane, left-to-right view (L–R).

visualize scientific data sets obtained using different rendering methods (see http://www.amira.com). Both pre- and postcontrast rat brain images were manually trimmed to exclude nonbrain structures. An ΔR_2 map according to Eq. (1) was calculated on a pixel-by-pixel basis using in-house software written in Matlab (MathWorks, Natick, MA). 3DΔR_2-mMRA involves constructing high-resolution 3D ΔR_2 maps using a VR or MIP utility (Amira, TGS). In the stroke model, paired *t*-test was used to compare the changes in ΔR_2 values between ipsilateral and contralateral side, with the significant level set at $P<0.05$.

Results

Fig. 1 shows axial ΔR_2 images with an in-plane resolution of 54.68 μm and a through-plane resolution of 72.91 μm (Fig. 1C) obtained from different locations of an entire 3D data set that was calculated from precontrast (Fig. 1A) and postcontrast (Fig. 1B) T2WI images according to Eq. (1). 3DΔR_2-mMRA was performed by reconstructing high-resolution 3D ΔR_2 images using a VR technique, as shown in dorsal (Figs. 2A and B) and lateral (Fig. 2C) views. Veins as well as all major venous sinuses and their ramifications were clearly visible on the brain surface. These vessels were further validated and identified in accordance with the cerebral vascular atlas (Scremin, 1995; Dorr et al., 2007) in the dorsal and lateral views as follows: superior olfactory sinus, superior cerebral veins, superior sagittal sinus, and caudal rhinal vein in the cerebrum (Figs. 2A and C); superior cerebellar vein, inferior cerebellar vein, and vertebral vein in the cerebellum (Fig. 2B); and the transverse sinus in the border between the cerebrum and cerebellum (Fig. 2B). The vessels on the brain surface were well correlated with vascular photographs obtained from dorsal bird's-eye and lateral views in the same rat, and their sizes were comparable between the proposed method and corresponding vascular photographs (Fig. 2D). The ratio of the diameters of vessels detected using the two methods was measured for selected vessels following coregistration as shown in Fig. 2D, which revealed that rendered vessels were on average 1.17-fold larger than those on vascular photographs. The architecture of small vessels including arterioles and venules inside the brain could be delineated by rendering ΔR_2-mMRA data along the three orthogonal views (Fig. 3), which illustrated the rich and complicated small-vessel structure in the rat brain, including the superficial intracortical and the deeper subcortical microvasculature. These results demonstrate the capability of the proposed method in visualizing cerebral small vessels.

Fig. 4 compares visualizations of the microvasculature between the presented method and the current widely used TOF-MRA. The images for these two methods were acquired from the same subject with an identical view, slab position, and image resolution. The figure indicates that many of the cerebral small vessels were more visible in 3DΔR_2-mMRA, with only major arteries being evident in TOF-MRA.

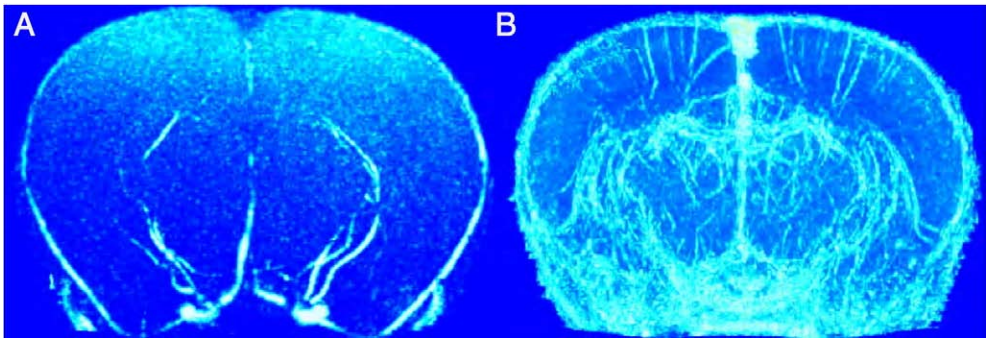

Fig. 4. Comparison between 3D MIP of (A) TOF-MRA and (B) ΔR_2-mMRA with identical axial view and slab region. The smaller vessels such as arterioles and venules appear to be most visible with theΔR_2-mMRA technique.

Please cite this article as: Lin, C.-Y., et al., In vivo cerebromicrovasculatural visualization using 3D ΔR_2-based microscopy of magnetic resonance angiography (3DΔR_2-mMRA), NeuroImage (2009), doi:10.1016/j.neuroimage.2008.12.030

A three-vessel occlusion stroke model was used to validate the capability of 3DΔR_2-mMRA in evaluating alterations to the microvasculature. Figs. 5A and B show VR of 3D high-resolution T2WI images and 3DΔR_2-mMRA data at 7 days after the reperfusion of a rat subjected to 60 min of MCA occlusion. T2WI images in different coronal views were extracted from a 3D data set with an in-plane resolution of 54.68 μm and a slice thickness of 500 μm (Fig. 5C). Fig. 5D shows the VR of 3DΔR_2-mMRA for the same slice position as in Fig. 5C. A much capillary-like brighter signal extending from the leptomeninges into the cortex were evident within the ipsilateral reperfused cortex. These results are consistent with the reports of (Lin et al., 2002, 2008), and further demonstrate that microvascular remodeling can be better visualized by the currently proposed 3DΔR_2-mMRA method. Quantitative analysis indicated that the ΔR_2 value was significantly higher within the ipsilateral reperfused cortex than within the contralateral cortex (Fig. 5E), but that no differences were evident between the hemispheres in subcortical regions. This finding agrees with previous evidence of an increased CBV due to ischemia-induced angiogenesis (Lin et al., 2002, 2008).

Discussion

Many studies have assessed the macro- and microvascular structure and function in cerebrovascular disease using either MRA techniques to visualize the vasculature (Reese et al., 1999; Miraux et al., 2004), or MR perfusion method to measure the hemodynamic parameters of CBV, cerebral blood flow (CBF), and permeability (Kastrup et al., 1999; Lin et al., 2002). The present study investigated a new approach of CBV-based

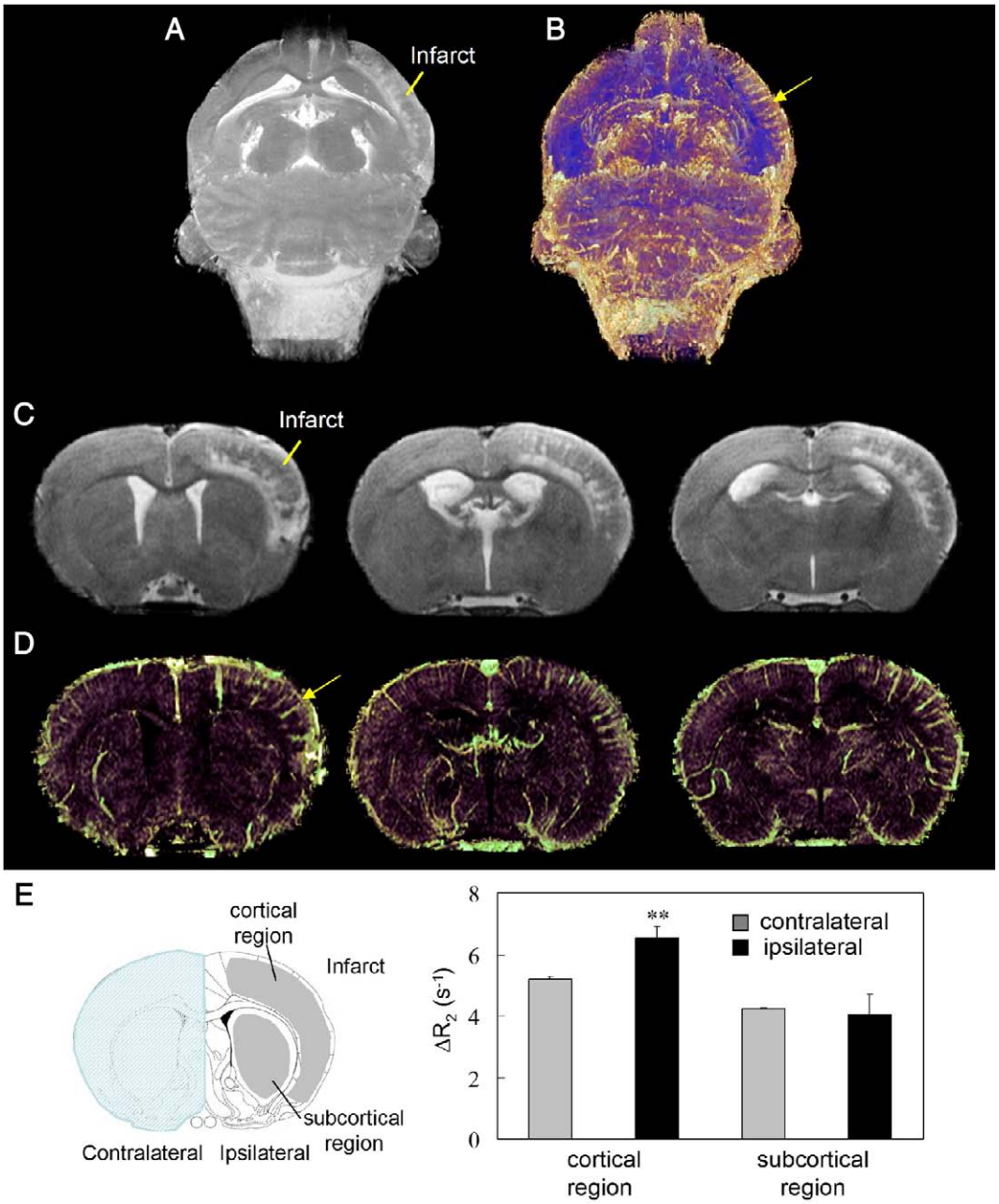

Fig. 5. T2WI and 3DΔR_2-mMRA images in a three-vessel occlusion ischemia model. (A) Dorsal view of VR 3D T2WI with a small angular tilt. (B) Dorsal view of VR 3DΔR_2-mMRA with a small angular tilt. (C) Selected multislice T2WI coronal sections depicting the infarct region in the right cortex. (D) Selected multislice 3DΔR_2-mMRA at the same position as C showing the changes in vascular morphology due to ischemia-induced angiogenesis within the infarct region. (E) Rat brain atlas and the regions selected for statistical analysis (left), and the differences in ΔR_2 value (right). Paired *t*-test indicated that the ΔR_2 value in the cortex was significantly higher on the ipsilateral side than on the contralateral side, while no differences were found in the subcortical region. ** indicates $P<0.01$, and error bars show s.e.m. values.

Please cite this article as: Lin, C.-Y., et al., In vivo cerebromicrovasculatural visualization using 3D ΔR_2-based microscopy of magnetic resonance angiography (3DΔR_2-mMRA), NeuroImage (2009), doi:10.1016/j.neuroimage.2008.12.030

Table 1
Comparison of commonly used MRA techniques

Parameters	MRA methods					
	TOF-MRA	CE-MRA	PC-MRA	Venography	Microangiography	ΔR_2-mMRA
Scanning sequence	GE	GE	GE	GE	GE	SE
Contrast of vasculature	Positive	Positive	Negative and positive	Negative	Positive	Positive
Visible vessels	Artery and fast-flow vein	Artery and vein	Artery and vein	Vein and venules	Artery, vein, venules and arterioles	Vein, venules and arterioles
Provided vascular function	Flow		Flow			Blood volume
Reference	Reese et al. (1999)	Miraux et al. (2004)	Dumoulin et al. (1989)	Reichenbach et al. (1997)	Bolan et al. (2006)	

TOF, time-of-flight; PC, phase contrast; GE, gradient echo; SE, spin echo.

microscopic MRA (3DΔR_2-mMRA), which is able to simultaneously reveal the morphology of the microvasculature and elucidate the physiological status of microvascular CBV. This new technique might greatly enhance our understanding of the development and treatment of cerebromicrovascular diseases such as strokes and brain tumors.

The current widely used MRA and proposed 3DΔR_2-mMRA methods are compared in Table 1. TOF-MRA is sensitive to the rapidly inflowing spins inside arteries, whereas CE-MRA employs contrast agents to detect vessels with high and low flow rates. Another technique is phase-contrast MRA (PC-MRA), which is based on calculating the phase shift, from which the velocity map is obtained by applying a suitable velocity-encoding value (Dumoulin et al., 1989). Vessels appear in TOF- and CE-MRA as positive signals, whereas vessels with inflow and outflow are distinguishable by PC-MRA as positive and negative signals, respectively. Although these methods can be used to visualize major arteries and veins, they have limited capabilities at imaging cerebral small vessels. In contrast, MR venography using susceptibility-weighted imaging (SWI) is able to detect venous vessels due to the presence of paramagnetic deoxyhemoglobin. However, although the visibility of venous vessel is increased by applying SWI, cerebral small vessels with higher oxygenation levels such as arterioles cannot be delineated. The method proposed here can in principle not only visualize venules but also depict arterioles (see Fig. 6) consistent with the vascular atlas of the rat brain (Scremin, 1995).

An alternative method based on gradient-echo images using the subtraction of pre- and postcontrast T2*WI images has been proposed for microangiography (Bolan et al., 2006). That study combined TOF-MRA with an iron-oxide contrast agent to reveal numerous penetrating and deep-branching vessels in the cat visual cortex. Their major contribution was distinguishing intracortical arterioles and venules; however, some aspects may need to be further investigated. First, the vessel size is usually overestimated using T2*WI due to both intra- and extravascular dephasing (Ogawa and Lee, 1990). Park et al. (2008) reported that the venous lumen diameter calculated from T2*WI appears to be three times larger than the actual vessel size. Note that the spatial extent of signal dephasing is dependent on the TE, field strength, and spatial resolution (Ogawa and Lee, 1990, Ogawa et al., 1990). Second, the vasculature cannot be clearly delineated by T2*WI in numerous brain regions — such as the amygdala in the rat brain and the temporal lobe in the human brain — due to strong susceptibility artifacts.

Another possible method for visualizing small vessels is high-resolution dynamic susceptibility contrast imaging (DSC), which is based on measuring the change in the T2 or T2* decrease during the first pass of an exogenous endovascular tracer through a capillary bed (Grandin, 2003). It can depict arteries and veins quite well, and can be used to derive perfusion parametric maps such as of the CBV and the mean transient time. A high resolution is required in all three spatial directions to visualize small vessels. However, DSC tends to maintain a high in-plane resolution but sacrifices the through-plane resolution in order to achieve a reasonable SNR when acquiring images with a high temporal resolution. Furthermore, visualizing small vessels at a high resolution using gradient echo and an echo planar imaging sequence would encounter problems of overestimating vessel sizes, strong susceptibility artifacts, and severe geometry distortion.

The proposed spin-echo-based 3DΔR_2-mMRA method can visualize the cerebral vasculature in the entire brain more homogeneously since it is subject to minimal susceptibility artifacts. In addition, the extravascular dephasing caused by the contrast agent can be significantly reduced, which means that vessel lumen sizes are detected more accurately (Ogawa et al., 1990, Ogawa et al., 1993, Boxerman et al., 1995). The rendered vessels from 3DΔR_2-mMRA on the brain surface were on average 1.17 larger than the actual sizes, which is at least two times better than the error when using the gradient-echo-based method (Park et al., 2008). This 17% overestimation of the vessel size is probably due to the partial volume effect. Furthermore, ΔR_2-mMRA directly indicates changes in transverse relaxivity within vessels, thus making it possible to measure the CBV. This means that the proposed method can be used to visualize the vascular morphology and the brain functional parameter simultaneously.

3DΔR_2-mMRA can be used to visualize both cerebral large vessels (e.g., veins and in sinuses, though with the exception of arteries) and cerebral small vessels (e.g., arterioles, and venules). This is believed to be due to the spin-echo-based ΔR_2 signal mainly consisting of IV and EV components. The specificity and sensitivity of IV and EV effects for various vessel sizes in gradient-echo- and spin-echo-based sequences have been described previously (Ogawa et al., 1993, Weisskoff et al., 1994, Boxerman et al., 1995, Duong et al., 2003). Briefly, the IV effect from spin-echo-based ΔR_2 occurs in vessels of all sizes, but it can be small within very large arteries due to the presence of a high flow rate, and the EV effect of ΔR_2 is associated with capillaries, which generally have diameters of less than 10 μm. The in-plane resolution of the proposed method can reach 54 μm with a total acquisition time of 76 min by using a 3D FSE sequence with an ETL of 32. Although this resolution is still larger than capillary diameters, it could be improved by increasing the imaging sensitivity in combination with a larger matrix and reduced FOV by using other rapid acquisition techniques such as parallel imaging (Madore and Pelc, 2001) or a more sophisticated coil design (Logothetis et al., 2002, Lee et al., 2005).

TOF-MRA and CE-MRA has been used to successfully evaluate MCA vascular occlusion and reperfusion (Beckmann et al., 1999, Besselmann et al., 2001), but it might not be suitable for investigating postischemic

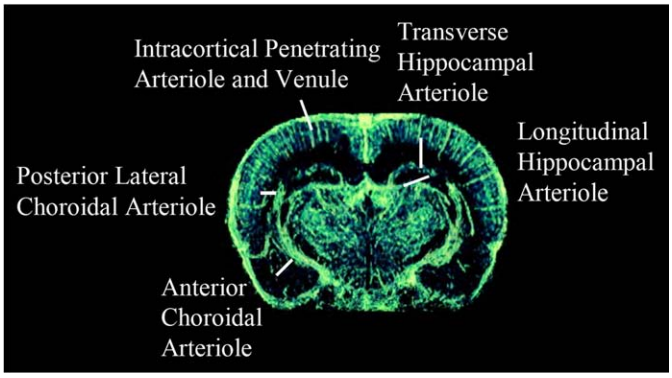

Fig. 6. VR 3DΔR_2-mMRA of a normal rat showing a 1-mm-thick coronal view taken from the entire 3D dataset. Small vascular structures in the cortical and deep brain are indicated.

Please cite this article as: Lin, C.-Y., et al., In vivo cerebromicrovasculatural visualization using 3D ΔR_2-based microscopy of magnetic resonance angiography (3DΔR_2-mMRA), NeuroImage (2009), doi:10.1016/j.neuroimage.2008.12.030

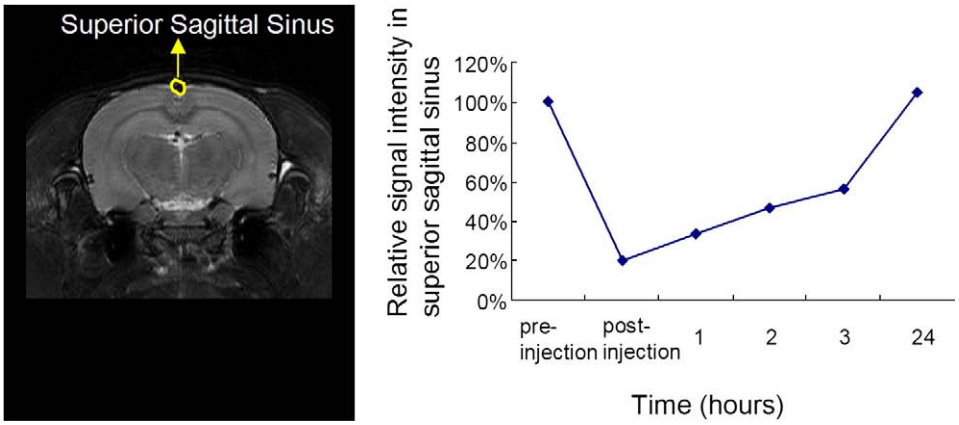

Fig. 7. Temporal signal changes in T2WI within a blood vessel of the superior sagittal sinus. The T2WI image was obtained with an FSE sequence with TR = 4000 ms and TE = 70 ms.

angiographic processes over time after reperfusion due to its limited ability to visualize small vessels. Vascular photographs from a dorsal bird's-eye view are commonly used to evaluate morphological changes on the brain surface in postischemic angiogenesis. However, the intracortical microvascular remodeling within a lesion side (rather than on the brain surface) is very difficult to visualize by vascular photography. Furthermore, it is difficult to examine an ischemic area immunohistologically due to liquefaction of brain tissue within an infarct region, especially more than 3 days after reperfusion. The changes in CBV and CBF measured by perfusion MR imaging within an infarct region in the chronic stage of ischemia have been documented (Lin et al., 2002). Although information on microvascular perfusion can be described by both of CBV and CBF, individual vessels cannot be discerned. Our novel 3DΔR_2-mMRA technique visualizes cerebral small vessels with high contrast and provides relative CBV mapping are able to simultaneously observe the morphological and hemodynamic changes in microvascular remodeling over time. In the present study, 3DΔR_2-mMRA revealed hyperintensities in the ipsilateral cortex after transient ischemia (Fig. 5), suggesting an increase in CBV as reported previously (Lin et al., 2002, 2008). 3DΔR_2-mMRA produced high-resolution images of small vessels extending from the leptomeninges into the cortex within the ischemic cortex. It is very likely that the newly formed small vessels were from the leptomeninges. This is the first MRA method that can reveal in vivo microangiographic processes in an ischemia model. This method is capable of tracing angiogenesis at different disease stages even in the presence of strong tissue necrosis within the lesion area.

The relative CBV is proportional to the ΔR_2 value (Wu et al., 2003, Dunn et al., 2004). However, the relative CBV can only be accurately measured when the contrast agent is in a steady-state condition in IV space. Since Resovist was used in the present study, we further evaluated changes in image intensity within blood vessels induced by Resovist over time. Fig. 7 shows the signal intensities in a brain vessel of the superior sagittal sinus prior to and after the injection of Resovist. The image intensity falls off rapidly (from 100% to 20%) immediately after the injection of Resovist, and then becomes relatively stable with a small linear increase during the first 3 hours (from 35% to 55%). Although the distribution of the Resovist in the blood vessel circulation was relatively stable when acquiring 3DΔR_2-mMRA images during the 76-min scanning time, changes in Resovist-related signals within the vessels might still need to be considered during image acquisition. Precise ΔR_2 quantification requires this change over time in k-space to be accounted for. The use of specialized contrast agents with high relaxivity and a prolonged half-life in vessels will help to increase the precision of ΔR_2 values and the microvasculature visibility when using contrast agent at lower concentrations in 3DΔR_2-mMRA.

The proposed technique represents a simple and novel approach that is easy to implement on a clinical scanner. However, several factors might need to be considered when applying this technique to humans. First, since the vessel signals of ΔR_2-mMRA are associated with contrast-agent-related susceptibility and both the susceptibility effect and the SNR are proportional to the magnetic field strength, the visibility of small vessels might increase with the magnetic field. Second, specific absorption rate limitations are frequently encountered when acquiring images using FSE with a high ETL, especially in high magnetic field. This could be accommodated by applying an FSE sequence with a variable flip-angle echo train (Naganawa et al., 2004), since this can significantly reduce RF power deposition. Third, a high resolution, adequate SNR, and reasonable scanning time are necessary for visualizing small vessels. High-resolution FSE imaging can be achieved using a strong gradient and fast slew rate. Since the gradient set with a smaller diameter will have higher gradient strength and faster slew rate, it is preferable to use dedicated smaller-diameter inserted gradients for head-only, rather than clinical body gradient sets. The SNR can be improved either by imaging with a high field strength or with a more efficient RF coil, such as a phased-array head coil (Roemer et al., 1990). The scanning time can be further reduced by utilizing recent developments in parallel imaging techniques (Madore and Pelc, 2001). Nevertheless, the technique requires a phased-array coil and multiple receiver channels, which might not be available for general clinical use.

Conclusions

We have described a steady-state ΔR_2-based and flow-independent microscopic MRA method combined with 3D image reconstruction techniques for the in vivo visualization of the architecture of small vessels of the rat brain. The method simultaneously provides high-resolution 3D information on the cerebral anatomy, in vivo micro-vascular architecture, and CBV mapping, which can be used to evaluate pathological microvascular changes over time. The technique might be suitable for use as a routine tool for examining the microvasculature in small-animal models and clinical patients who are healthy or are affected by cerebrovascular disease.

Acknowledgments

The authors acknowledge technical support from the Functional and Micro-Magnetic Resonance Imaging Center supported by the National Research Program for Genomic Medicine, National Science Council, Taiwan, ROC (NSC97-3112-B-001-013). We gratefully thank the helpful discussion of Dr. Yen-Yu Shih.

Please cite this article as: Lin, C.-Y., et al., In vivo cerebromicrovasculatural visualization using 3D ΔR_2-based microscopy of magnetic resonance angiography (3DΔR_2-mMRA), NeuroImage (2009), doi:10.1016/j.neuroimage.2008.12.030

References

Bandettini, P.A., Wong, E.C., 1995. Effects of biophysical and physiologic parameters on brain activation-induced R_2* and R_2 changes: simulation using a deterministic diffusion model. Int. J. Imaging Syst. Techol. 6, 133–152.

Beckmann, N., 2000. High resolution magnetic resonance angiography non-invasively reveals mouse strain differences in the cerebrovascular anatomy in vivo. Magn. Reson. Med. 44, 252–258.

Beckmann, N., Stirnimann, R., Bochelen, D., 1999. High-resolution magnetic resonance angiography of the mouse brain: application to murine focal cerebral ischemia models. J. Magn. Reson. 140, 442–450.

Besselmann, M., Liu, M., Diedenhofen, M., Franke, C., Hoehn, M., 2001. MR angiographic investigation of transient focal cerebral ischemia in rat. NMR Biomed. 14, 289–296.

Bolan, P.J., Yacoub, E., Garwood, M., Ugurbil, K., Harel, N., 2006. In vivo micro-MRI of intracortical neurovasculature. NeuroImage 32, 62–69.

Boxerman, J.L., Hamberg, L.M., Rosen, B.R., Weisskoff, R.M., 1995. MR contrast due to intravascular magnetic susceptibility perturbations. Magn. Reson. Med. 34, 555–566.

Brubaker, L.M., Bullitt, E., Yin, C., Van Dyke, T., Lin, W., 2005. Magnetic resonance angiography visualization of abnormal tumor vasculature in genetically engineered mice. Cancer Res. 65, 8218–8223.

Buee, L., Hof, P.R., Delacourte, A., 1997. Brain microvascular changes in Alzheimer's disease and other dementias. Ann. N.Y. Acad. Sci. 826, 7–24.

Cai, W., Sakas, G., 1998. Maximum intensity projection using splatting in sheared object space. Comput. Graph. Forum 17, 113–124.

Dennie, J., Mandeville, J.B., Boxerman, J.L., Packard, S.D., Rosen, B.R., Weisskoff, R.M., 1998. NMR imaging of changes in vascular morphology due to tumor angiogenesis. Magn. Reson. Med. 40, 793–799.

Dorr, A., Sled, J.G., Kabani, N., 2007. Three-dimensional cerebral vasculature of the CBA mouse brain: a magnetic resonance imaging and micro computed tomography study. NeuroImage 35, 1409–1423.

Drebin, R., Carpenter, L., Harrahan, P., 1988. Volume rendering. SIGGRAPH 88, 665–674.

Dumoulin, C.L., Souza, S.P., Walker, M.F., Wagle, W., 1989. Three-dimensional phase contrast angiography. Magn. Reson. Med. 9, 139–149.

Dunn, J.F., Roche, M.A., Springett, R., Abajian, M., Merlis, J., Daghlian, C.P., Lu, S.Y., Makki, M., 2004. Monitoring angiogenesis in brain using steady-state quantification of ΔR_2 with MION infusion. Magn. Reson. Med. 51, 55–61.

Duong, T.Q., Yacoub, E., Adriany, G., Hu, X., Ugurbil, K., Kim, S.G., 2003. Microvascular BOLD contribution at 4 and 7 T in the human brain: gradient-echo and spin-echo fMRI with suppression of blood effects. Magn. Reson. Med. 49, 1019–1027.

Grandin, C.B., 2003. Assessment of brain perfusion with MRI: methodology and application to acute stroke. Neuroradiology 45, 755–766.

Kastrup, A., Engelhorn, T., Beaulieu, C., de Crespigny, A., Moseley, M.E., 1999. Dynamics of cerebral injury, perfusion, and blood–brain barrier changes after temporary and permanent middle cerebral artery occlusion in the rat. J. Neurol. Sci. 166, 91–99.

Koopmans, P.J., Manniesing, R., Niessen, W.J., Viergever, M.A., Barth, M., 2008. MR venography of the human brain using susceptibility weighted imaging at very high field strength. Magma 21, 149–158.

Lee, H.L., Lin, I.T., Chen, J.H., Horng, H.E., Yang, H.C., 2005. High-T-c superconducting receiving coils for nuclear magnetic resonance imaging. IEEE Trans. Appl. Supercond. 15, 1326–1329.

Lei, H., Grinberg, O., Nwaigwe, C.I., Hou, H.G., Williams, H., Swartz, H.M., Dunn, J.F., 2001. The effects of ketamine–xylazine anesthesia on cerebral blood flow and oxygenation observed using nuclear magnetic resonance perfusion imaging and electron paramagnetic resonance oximetry. Brain Res. 913, 174–179.

Lin, T.N., He, Y.Y., Wu, G., Khan, M., Hsu, C.Y., 1993. Effect of brain edema on infarct volume in a focal cerebral ischemia model in rats. Stroke 24, 117–121.

Lin, T.N., Sun, S.W., Cheung, W.M., Li, F., Chang, C., 2002. Dynamic changes in cerebral blood flow and angiogenesis after transient focal cerebral ischemia in rats. Evaluation with serial magnetic resonance imaging. Stroke 33, 2985–2991.

Lin, C.Y., Chang, C., Cheung, W.M., Lin, M.H., Chen, J.J., Hsu, C.Y., Chen, J.H., Lin, T.N., 2008. Dynamic changes in vascular permeability, cerebral blood volume, vascular density, and size after transient focal cerebral ischemia in rats: evaluation with contrast-enhanced magnetic resonance imaging. J. Cereb. Blood Flow Metab. 28, 1491–1501.

Logothetis, N., Merkle, H., Augath, M., Trinath, T., Ugurbil, K., 2002. Ultra high-resolution fMRI in monkeys with implanted RF coils. Neuron 35, 227–242.

Madore, B., Pelc, N.J., 2001. SMASH and SENSE: experimental and numerical comparisons. Magn. Reson. Med. 45, 1103–1111.

Miraux, S., Serres, S., Thiaudiere, E., Canioni, P., Merle, M., Franconi, J.M., 2004. Gadolinium-enhanced small-animal TOF magnetic resonance angiography. Magma 17, 348–352.

Naganawa, S., Kawai, H., Fukatsu, H., Ishigaki, T., Komada, T., Maruyama, K., Takizawa, O., 2004. High-speed imaging at 3 Tesla: a technical and clinical review with an emphasis on whole-brain 3D imaging. Magn. Reson. Med. Sci. 3, 177–187.

Ogawa, S., Lee, T.M., 1990. Magnetic resonance imaging of blood vessels at high fields: in vivo and in vitro measurements and image simulation. Magn. Reson. Med. 16, 9–18.

Ogawa, S., Lee, T.M., Nayak, A.S., Glynn, P., 1990. Oxygenation-sensitive contrast in magnetic resonance image of rodent brain at high magnetic fields. Magn. Reson. Med. 14, 68–78.

Ogawa, S., Menon, R.S., Tank, D.W., Kim, S.G., Merkle, H., Ellermann, J.M., Ugurbil, K., 1993. Functional brain mapping by blood oxygenation level-dependent contrast magnetic resonance imaging. A comparison of signal characteristics with a biophysical model. Biophys. J. 64, 803–812.

Park, S.H., Masamoto, K., Hendrich, K., Kanno, I., Kim, S.G., 2008. Imaging brain vasculature with BOLD microscopy: MR detection limits determined by in vivo two-photon microscopy. Magn. Reson. Med. 59, 855–865.

Perlmutter, L.S., Chui, H.C., 1990. Microangiopathy, the vascular basement membrane and Alzheimer's disease: a review. Brain Res. Bull. 24, 677–686.

Pipe, J.G., 2001. Limits of time-of-flight magnetic resonance angiography. Top. Magn. Reson. Imaging 12, 163–174.

Reese, T., Bochelen, D., Sauter, A., Beckmann, N., Rudin, M., 1999. Magnetic resonance angiography of the rat cerebrovascular system without the use of contrast agents. NMR Biomed. 12, 189–196.

Reichenbach, J.R., Venkatesan, R., Schillinger, D.J., Kido, D.K., Haacke, E.M., 1997. Small vessels in the human brain: MR venography with deoxyhemoglobin as an intrinsic contrast agent. Radiology 204, 272–277.

Roemer, P.B., Edelstein, W.A., Hayes, C.E., Souza, S.P., Mueller, O.M., 1990. The NMR phased array. Magn. Reson. Med. 16, 192–225.

Scremin, O.U., 1995. Cerebral vascular system. In: Paxions, G. (Ed.), The Rat Nervous System. Academic Press, San Diego, pp. 3–35.

Serne, E.H., de Jongh, R.T., Eringa, E.C., RG, I.J., Stehouwer, C.D., 2007. Microvascular dysfunction: a potential pathophysiological role in the metabolic syndrome. Hypertension 50, 204–211.

van Vliet, M., van Dijke, C.F., Wielopolski, P.A., ten Hagen, T.L., Veenland, J.F., Preda, A., Loeve, A.J., Eggermont, A.M., Krestin, G.P., 2005. MR angiography of tumor-related vasculature: from the clinic to the micro-environment. Radiographics 25 (Suppl. 1), S85–97 discussion S97-88.

Weisskoff, R.M., Zuo, C.S., Boxerman, J.L., Rosen, B.R., 1994. Microscopic susceptibility variation and transverse relaxation: theory and experiment. Magn. Reson. Med. 31, 601–610.

Wu, E.X., Wong, K.K., Andrassy, M., Tang, H., 2003. High-resolution in vivo CBV mapping with MRI in wild-type mice. Magn. Reson. Med. 49, 765–770.

Please cite this article as: Lin, C.-Y., et al., In vivo cerebromicrovasculatural visualization using 3D ΔR_2-based microscopy of magnetic resonance angiography (3DΔR_2-mMRA), NeuroImage (2009), doi:10.1016/j.neuroimage.2008.12.030